

# Enhancement of Mechanical Properties and Corrosion Resistance of Ultra-Fine Grain $\text{Al}_{0.4}\text{FeCrCo}_{1.5}\text{NiTi}_{0.3}$ High-Entropy Alloy by MA and SPS Technologies

Shaofeng YANG<sup>1,2\*</sup>, Yan ZHANG<sup>1,2</sup>, Xing YAN<sup>2</sup>, Hang ZHOU<sup>2</sup>

<sup>1</sup> Jiangsu Key Laboratory of Advanced Structural Materials and Application Technology, Nanjing, 211167, China

<sup>2</sup> School of Materials Science and Engineering, Nanjing Institute of Technology, Nanjing, 211167, China

**crossref** <http://dx.doi.org/10.5755/j01.ms.25.3.19452>

Received 10 November 2017; accepted 30 March 2018

$\text{Al}_{0.4}\text{FeCrCo}_{1.5}\text{NiTi}_{0.3}$  high-entropy alloy (HEA) was prepared by mechanical alloying (MA) and spark plasma sintering (SPS), which were evaluated in this study by XRD and TEM. After SPS, the bulk alloy exhibited a structure with a dominant fcc phase, a minor volume fraction of bcc phase, and the formation of  $\text{TiAl}_3$  intermetallic compound. Deformation twinning was observed in the fcc phase in the bulk HEA. The latter had a compressive strength, strain and Vickers hardness of  $2225 \pm 15$  MPa,  $17.52 \pm 0.50$  % and  $515 \pm 16$  HV, respectively. The corrosion resistance studies indicated that  $\text{Al}_{0.4}\text{FeCrCo}_{1.5}\text{NiTi}_{0.3}$  with ultra-fine grained micro-structure was easier to passivate and possessed excellent corrosion resistance.

**Keywords:** high-entropy alloy, powder metallurgy, TEM, micro-structure properties.

## 1. INTRODUCTION

In the last decade, high-entropy alloys (HEAs) have been increasing in popularity [1-3]. According to the principles of maximum entropy production, the multi-principal element alloys can form only simple phases of solid solutions [3, 4]. Several researchers have reported that HEAs display superior anticorrosive properties, high hardness and strength, which offer great potential for industrial applications [5].

The processing techniques for bulk HEA fabrication include arc-melting/casting [5], Bridgman solidification [6], mechanical alloying (MA), and powder sintering. The latter, in turn, includes spark plasma sintering (SPS) [7, 8]. By comparison, mechanical alloying combined with powder sintering may provide a preferential potential method for industrial component fabrication. Al and Ti have larger atomic radii than other constituents and are conducive to lattice distortion, which results in higher strength and hardness but less plasticity. On the other hand, Cu, Co and Ni, which have smaller atomic radii, can be used to produce HEAs with the desired plasticity. Therefore, in this study, an  $\text{Al}_{0.4}\text{FeCrCo}_{1.5}\text{NiTi}_{0.3}$  alloy with Al, Ti and high Co contents was fabricated using the MA and SPS techniques and its microstructure and properties were investigated in detail.

## 2. EXPERIMENTAL

$\text{Al}_{0.4}\text{FeCrCo}_{1.5}\text{NiTi}_{0.3}$  HEA, with the nominal composition as expressed in the molar ratio, was prepared by dry milling the constituents for 50h and subsequent wet milling for 5h in ethanol. All elemental powders had purity exceeding 99.9 wt.% and particle sizes  $\leq 50$   $\mu\text{m}$ . The milling was carried out in high energy QM-3SP4 planetary ball mill in an argon atmosphere with mill rotational speed

300 rpm and a ball for the achieved powder weight ratio of 10:1. The alloy powder was ball-milled for 50h and dried for 48 h and subsequently was compacted by SPS (Sum. Co. Min Co. Ltd., Japan) at 1273 K for 10 min at 30 MPa pressure in vacuum.

The milled powders and bulk specimens produced by SPS were analyzed using a Bruker D8 ADVANCE X-ray diffractometer, as well as with a Nova nano SEM430 scanning electron microscope (SEM) and a transmission electron microscope (TEM) (JEM-2100). The compressive properties of the specimens ( $\varnothing 3$  mm  $\times$  4.5 mm in size) were evaluated using a compression testing system. The corrosion resistance was evaluated with immersion tests and potentiodynamic polarization measurements (calomel reference electrode, 1mol/L NaOH solution, scanning speed 5 mv/s and an effective area of 1  $\text{cm}^2$ ).

## 3. RESULTS AND DISCUSSION

The XRD patterns of  $\text{Al}_{0.4}\text{FeCrCo}_{1.5}\text{NiTi}_{0.3}$  high-entropy alloy are depicted in Fig. 1. Pure Al, Fe, Cr, Co, Ni and Ti were mixed before milling (0 h). After milling for 10 h, the mixed powder comprised solid solutions with fcc and bcc phases. When the milling time was extended to 50 h, broader diffraction peaks were evident for the powder, indicating a finer grain structure, as compared to that of powder milled for 10 h. According to the Scherrer formula:

$$D = K\lambda/(\beta\cos\theta), \quad (1)$$

where  $D$  is the mean size of the ordered (crystalline) domains;  $K$  is a dimensionless shape factor (about 0.9);  $\lambda$  is the X-ray wavelength;  $\beta$  is the line broadening at half the maximum intensity after subtracting the instrumental line broadening, in radians; and  $\theta$  is the Bragg angle in degrees. From Eq. 1, the crystallite sizes and lattice strains of fcc and bcc phases in the powder milled for 50 h were estimated as 9.8 nm versus 9.5 nm, and 1.29 % versus

\* Corresponding author. Tel.: +86-25-86118274; fax: +86-25-86118271. E-mail address: yangshf@njit.edu.cn. (S.F. Yang)

0.89 %, respectively. The above results strongly suggest that the nanostructured HEA can be obtained using the MA process. The XRD pattern of Al<sub>0.4</sub>FeCrCo<sub>1.5</sub>NiTi<sub>0.3</sub> HEA after SPS (Fig. 1 a) indicated that the main phase of the bulk specimen was fcc phase, while several weak peaks corresponding to the TiAl<sub>3</sub> intermetallic compound appeared after SPS. The reordering, which facilitated the formation of metastable supersaturated solid solution by MA, resulted in appearance of more stable phases during the SPS process, which also may lead to transformation of the bcc phase into the more stable fcc structure, which was similar to the TiAl<sub>3</sub> intermetallic compound.

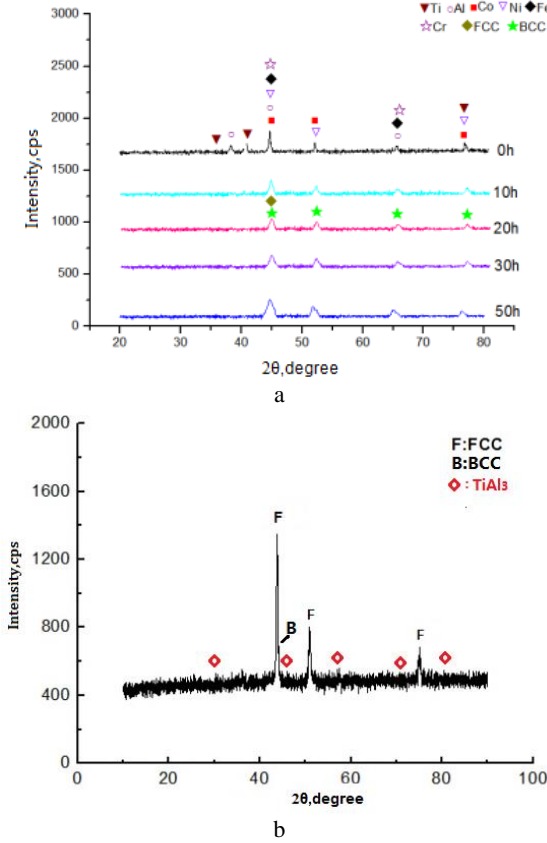


**Fig. 1.** a – XRD patterns of Al<sub>0.4</sub>FeCrCo<sub>1.5</sub>NiTi<sub>0.3</sub> high-entropy alloy for mechanically alloyed powders with different milling times; b – after SPS

According to Yang et al [9], the atomic size difference ( $\delta$ ), mixing enthalpy ( $\Delta H_{mix}$ ) commonly are used to characterize the collective behavior of the constituent elements in multi-component alloys. In addition, Yang et al [10] proposed that two factors control the stable solid-solution formation of multi-component HEAs, viz., the thermodynamic parameter  $\Omega \geq 1.1$  and atomic size difference  $\delta \leq 6.6\%$ . Mathematically, the parameters  $\Omega$  and  $\delta$  can be defined as follows:

The atomic size difference ( $\delta$ ) is defined as:

$$\delta = \sqrt{\sum_{i=1}^n c_i (1 - r_i / \bar{r})^2} \quad (2)$$

where  $c_i$  is the atomic percentage of the  $i_{th}$  component,  $\bar{r} = \sum_{i=1}^n c_i r_i$  is the average atomic radius, and  $r_i$  is the atomic radius of the  $i_{th}$  component.

The thermodynamic parameter ( $\Omega$ ) is derived as:

$$\Omega = \frac{T_m \Delta S_{mix}}{|\Delta H_{mix}|} \quad (3)$$

where  $T_m = \sum_{i=1}^n c_i (T_m)_i$ , and  $(T_m)_i$  is the melting point of the  $i_{th}$  component.

The mixing enthalpy ( $\Delta H_{mix}$ ) can be derived as:

$$\Delta H_{mix} = \sum_{i=1, i \neq j}^n \Omega_{ij} c_i c_j \quad (4)$$

where  $\Omega_{ij} (= 4\Delta H_{mix}^{ij})$  is the regular solution interaction parameter between the  $i_{th}$  and  $j_{th}$  elements,  $c_i$  and  $c_j$  are the atomic percentages of the  $i_{th}$  and  $j_{th}$  components, respectively. It is noteworthy is that the mixing enthalpy ( $\Delta H_{mix}^{ij}$ ) was assessed using the Miedema macroscopic model for binary liquid alloys, and hence the mixing entropy ( $\Delta S_{mix}$ ) can be written as:

$$\Delta S_{mix} = -R \sum_{i=1}^n c_i \ln c_i \quad (5)$$

where  $c_i$  is the component mole percent,  $\sum_{i=1}^n c_i = 1$ , and  $R$  ( $= 8.314 \text{ J}^{-1} \text{ K mol}^{-1}$ ) is the universal gas constant.

**Table 1.** The chemical mixing enthalpy ( $\Delta H_{mix}$ ,  $i_j$ ,  $\text{kJ mol}^{-1}$ ) of binary equi-atomic alloys.

Element (atomic sizes, Å)	Co	Fe	Ni	Cr	Al	Ti
Co (1.26)	–	–1	0	–4	–19	–28
Fe (1.27)	–	–	–2	–1	–11	–17
Ni (1.25)	–	–	–	–7	–22	–35
Cr (1.28)	–	–	–	–	–10	–7
Al (1.43)	–	–	–	–	–	–30
Ti (1.46)	–	–	–	–	–	–

The parameters  $\Delta S_{mix}$ ,  $\Delta H_{mix}$ ,  $T_m$ ,  $\delta$ , and  $\Omega$  for the Al<sub>0.4</sub>FeCrCo<sub>1.5</sub>NiTi<sub>0.3</sub> HEA reported were  $14.802 \text{ J mol}^{-1} \text{ K}^{-1}$ ,  $-15.745 \text{ KJ mol}^{-1}$ ,  $1783.71 \text{ K}$ ,  $6.54\%$  and  $1.68$ , respectively. A high value of entropy of mixing ( $\Delta S_{mix}$ ) is required for the formation of solid solutions, such as the bcc and fcc phases, during the MA process [11–13].

In this study, metastable supersaturated solid solution was formed during the MA process due to numerous defects introduced into the structure by the severe plastic deformation. However, these metastable supersaturated solid solutions were transformed into more stable phases, because the plastic deformation-induced defects were annihilated by annealing (1273 K for 10 min) during the SPS procedure [14]. The increased proportion of fcc phase indicated that densification by during SPS sintering gave rise to development of more stable phases.

SEM images of the bulk Al<sub>0.4</sub>FeCrCo<sub>1.5</sub>NiTi<sub>0.3</sub> consolidated by SPS are showed in Fig. 2. Only a few pores were observed in the consolidated specimen, as evident in Fig 2 a. Two distinctive areas of irregular bulk areas (Region 1) and small irregular areas (Region 2) can be observed in Fig. 2 b. The phases of Region 2 consisted

of ultra-fine grained structures, with a size of no more than 200 nm. This confirmed that nanostructured HEAs could be produced by short-time exposure SPS sintering at 1273 K.

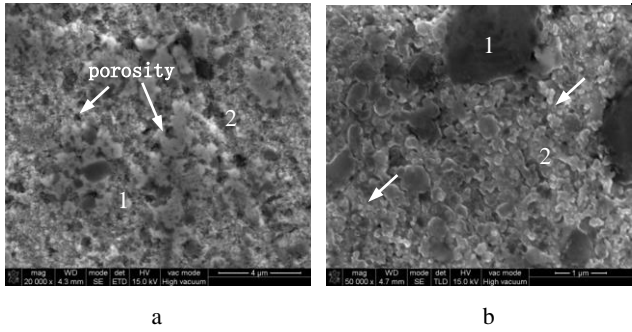


**Fig. 2.** SEM micrographs of bulk  $\text{Al}_{0.4}\text{FeCrCo}_{1.5}\text{NiTi}_{0.3}$  HEA: a – low-magnification; b – high-magnification

The appearance of bulk  $\text{Al}_{0.4}\text{FeCrCo}_{1.5}\text{NiTi}_{0.3}$  HEA after SPS is shown in Fig. 3. EDS/TEM analysis and SAED revealed the presence of the fcc phase structure. The composition analyses of the detailed phases that were obtained from EDS/TEM are summarized in Table 2 (at.%) and indicate that the primary fcc phase was enriched in Co, slightly enriched in Cr–Ni–Fe- and depleted in Al–Ti-. However, a small portion of bcc phase was Al–Ti-rich and slightly Co–Ni–Fe–Cr-rich. Several reports on the phenomenon of bcc phase being promoted by Al, Ti, etc., and on the fcc phase being promoted by Co, Ni, etc., are described elsewhere [18], demonstrating that HAE phases can be changed dramatically by adjusting the Al content. With an increase in the Al ( $0 \leq \text{Al} \leq 2$ ) content, the phases changed from fcc to bcc + fcc and then to bcc structures. In addition to the fcc and bcc phases, the composition of Regions 11 and 12 was enriched in Al–Ti and were depleted in Co–Ni–Fe–Cr. The content ratio of Al (69.5 at.%) and Ti (22.7 at.%) was close to 3:1, which implied that the phase was  $\text{TiAl}_3$ , as confirmed by the XRD results. The grain sizes of the phases varied in the range from several hundred nanometers to less than 200 nm.

In  $\text{Al}_{0.4}\text{FeCrCo}_{1.5}\text{NiTi}_{0.3}$  HEA, the fcc phase consisted mainly of Co, Fe, Cr and Ni, which have small and approximately identical atomic sizes (1.25 to 1.28), whereas the mixing enthalpy of atom-pairs for these four elements was close to  $0 \text{ kJmol}^{-1}$ , except for that of the Ni–Cr ( $-7 \text{ kJmol}^{-1}$ ). The fcc phase was (Co–Fe–Ni–Cr)-based phase, while the bcc phase was composed mainly of more Al and Ti. The mixing enthalpy of atom-pairs between the elements in the bcc phases varied from  $-11$  to  $-30 \text{ kJmol}^{-1}$ . It was noted that the  $\text{TiAl}_3$  phase also was formed in this alloy and the reaction between Ti and Al can be reduced to:



**Table 2.** Phases examined by EDS/TEM (at.%) according to Fig. 3

Regions	Phases	Al	Fe	Cr	Co	Ni	Ti
1, 6, 7	bcc	$21.8 \pm 0.5$	$14.9 \pm 0.4$	$16.2 \pm 0.7$	$20.7 \pm 0.8$	$15.7 \pm 0.6$	$13.7 \pm 0.2$
2, 3, 4, 5, 8, 9, 10	fcc	$3.9 \pm 0.5$	$20.1 \pm 0.5$	$24.2 \pm 0.5$	$29.4 \pm 0.5$	$20.8 \pm 0.5$	$1.7 \pm 0.5$
11, 12	$\text{TiAl}_3$	$69.5 \pm 0.30$	$1.4 \pm 0.1$	$1.7 \pm 0.2$	$1.8 \pm 0.1$	$1.5 \pm 0.2$	$22.7 \pm 2.4$

According to the Gibbs free energy concept,  $\Delta G = \Delta H - T\Delta S$ , while  $\Delta H$  for Al and Ti is  $-183 \text{ Jmol}^{-1}$ , and  $\Delta G = -115 \text{ Jmol}^{-1}$  at  $1200 \text{ }^\circ\text{C}$ . Hence, the formation of  $\text{TiAl}_3$  is quite possible in this system. The above results strongly suggest that the predominant fcc phase was promoted by the Co and Ni content of the alloy, with a small quantity of Al-rich bcc phase and small-scale  $\text{TiAl}_3$  phase.

Moreover, twins with a size of approximately  $200 \times 100 \text{ nm}$  are evident in Fig. 4. It should be noted that deformation nano-twins were observed only in the fcc phase. The matrix axis was  $[011]_M$  and the twin axis was  $[0\bar{1}\bar{1}]_r$ . The phase of the nano-twins was Co–Ni–Fe–Cr-rich and the lattice parameter was  $3.720 \text{ \AA}$ , which was approximately consistent with  $3.705 \text{ \AA}$  (fcc) based on the XRD results (Fig. 1). According to the SAED pattern, the diffraction spot of twinned fcc grains were deformed in the counter-clockwise direction of the (111) lattice plane. The calculated results, among other findings, imply that the  $(\bar{1}\bar{1}\bar{1})_r$  of the twinned fcc grain featured the removed  $-\frac{2}{3}(111)$  crystal lattice on the  $(1\bar{1}\bar{1})$  lattice spot along the (111) lattice plane. These  $\text{TiAl}_3$  phases were revealed from the EDS/TEM analyses, which indicated that the formation of  $\text{TiAl}_3$  phase could affect deformation twinning behavior (Region 1 in Fig. 4, and Regions 11 and 12 in Fig. 3 a).

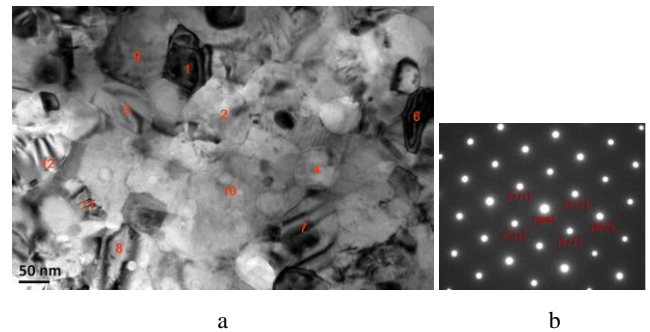


**Fig. 3.** TEM of bulk  $\text{Al}_{0.4}\text{FeCrCo}_{1.5}\text{NiTi}_{0.3}$ : a – bright field image; b – SAED pattern of fcc [011] zone axis (Region 10)

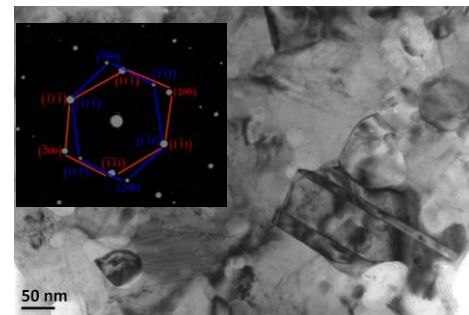


**Fig. 4.** TEM microstructure and SAED pattern of twinned fcc phase with corresponding SAED pattern along  $ZM = [011]_M$  and  $ZT = [0\bar{1}\bar{1}]_r$  zone axes

The TiAl<sub>3</sub> hard phase can be presumed to be a partial fcc phase with deformation nanoscale twins. Consequently, the fcc deformation nanoscale twins took a more stable form, attaining complete densification. Similar nano-twins have been observed in the some HEAs systems, which are reported elsewhere [15–17].

The compression curve of bulk Al<sub>0.4</sub>FeCrCo<sub>1.5</sub>NiTi<sub>0.3</sub> HEA is shown in Fig. 5. The yield strength ( $\sigma_y$ ), compressive strength ( $\sigma_{max}$ ) and compression strain ( $\epsilon_p$ ) are  $2012 \pm 20$  MPa,  $2225 \pm 15$  MPa and  $17.52 \pm 0.50$  %, respectively. The average Vickers hardness of Al<sub>0.4</sub>FeCrCo<sub>1.5</sub>NiTi<sub>0.3</sub> HEA after SPS was assessed as  $515 \pm 16$  HV. By comparison with the typical HEAs listed in Table 1, these results corroborated the excellent mechanical properties of the alloy under study. As shown in Table 3, the ultimate strain of Al<sub>0.4</sub>FeCrCo<sub>1.5</sub>NiTi<sub>0.3</sub> was very high, as compared to other HEAs. High compressive strength may result from solid-solution strengthening due to multi-elements in the main ductile fcc phase.

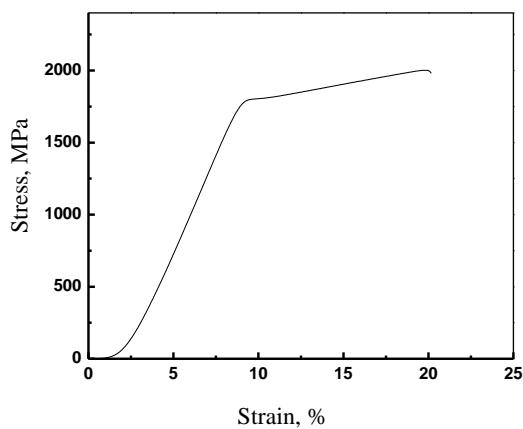


**Fig. 5.** Compression curve of Al<sub>0.4</sub>FeCrCo<sub>1.5</sub>NiTi<sub>0.3</sub>HEA

The corrosion tests were carried out in 1mol/L NaOH solution for 50 days' immersion period at 25 °C. Photographs of the corroded surface of bulk Al<sub>0.4</sub>FeCrCo<sub>1.5</sub>NiTi<sub>0.3</sub> HEA are shown in Fig. 6. The major type of corrosion was uniform corrosion, while some approximately spherical corrosion products could be observed on the surface. In addition, microcracks (marked by white arrows in Fig. 6) also were found. Three distinctive areas were readily observed from the high-magnification SEM image (Fig. 6 b), viz., gray background areas (Region 1), spherical corrosion product/debris areas (Region 2) and circular pitting (Region 3). Smaller spherical corrosion products/debris were found at the bottom of corrosion pits. The energy-dispersive investigation of the bulk Al<sub>0.4</sub>FeCrCo<sub>1.5</sub>NiTi<sub>0.3</sub> alloy indicated that the main elements of spherical corrosion

products (Region 2) were O, Al, Fe, Cr, Co, and Ni with approximately equal atomic percentages (in Fig. 7). This illustrates that the main corrosion products were oxides, such as Al<sub>2</sub>O<sub>3</sub>. Meanwhile, the main elements observed in the gray areas (Region 1) were O, Al and Ti with minor amounts of Fe, Cr, Co, and Ni. The following interpretation of the corrosion phenomena of the bulk Al<sub>0.4</sub>FeCrCo<sub>1.5</sub>NiTi<sub>0.3</sub> can be proposed. As known, a reaction can easily occur between Al and sodium hydroxide solution but not with any of the other elements mentioned. The reaction can be represented as follows:



where Na[Al(OH)<sub>4</sub>] is a metastable phase that finally is transformed to the stable product Al<sub>2</sub>O<sub>3</sub>, which can form a uniform nonprotective passive film on the bulk Al<sub>0.4</sub>FeCrCo<sub>1.5</sub>NiTi<sub>0.3</sub> surface. However, hydrogen also is formed on the surface and may produce gas pressure in the passivation layer, affecting the circular pitting areas. Consequently, this pressure will lead to a newly exposed surface of HEA alloy in the sodium hydroxide solution, with corrosion processes occurring in these areas. Thus, spherical corrosion products are formed at the bottom of corrosion pits, in accordance with Fig. 6 b (Region 3).

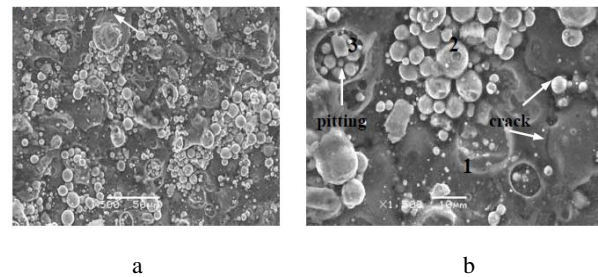


**Fig. 6.** a–low and b– high-magnification photographs of the corroded surface of bulk Al<sub>0.4</sub>FeCrCo<sub>1.5</sub>NiTi<sub>0.3</sub> HEA after SPS

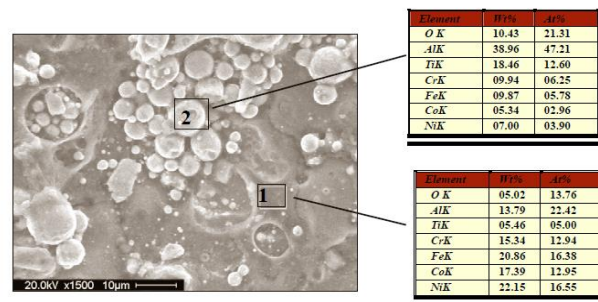


**Fig. 7.** The EDS analysis results for the corroded surface of bulk Al<sub>0.4</sub>FeCrCo<sub>1.5</sub>NiTi<sub>0.3</sub> HEA after SPS

**Table 3.** Mechanical properties of different HEAs according to compression test

HEAS	Process	$\sigma_y$ , MPa	$\sigma_{max}$ , MPa	$\epsilon_p$ , %	Hardness, HV	References
Al <sub>0.4</sub> FeCrCo <sub>1.5</sub> NiTi <sub>0.3</sub>	MA+SPS	$2012 \pm 20$	$2225 \pm 15$	$17.52 \pm 0.50$	$515 \pm 16$	This study
Al <sub>0.5</sub> CrFeNiCo <sub>0.3</sub> Co <sub>0.2</sub>	MA+SPS	–	2131	3.0	$617 \pm 25$	8
FeNiCrCo <sub>0.3</sub> Al <sub>0.7</sub>	MA+SPS	$2033 \pm 41$	$2635 \pm 55$	$8.12 \pm 0.51$	$624 \pm 26$	9
AlCoCrCuFeNiMo	Arc-melting	1750	2600	1.1	–	10
AlCoCrCuFeNi	Arc-melting	1300	2270	9.9	–	10
AlCoCrFeNiMo0.1	Arc-melting	957	2550	10.52	–	10

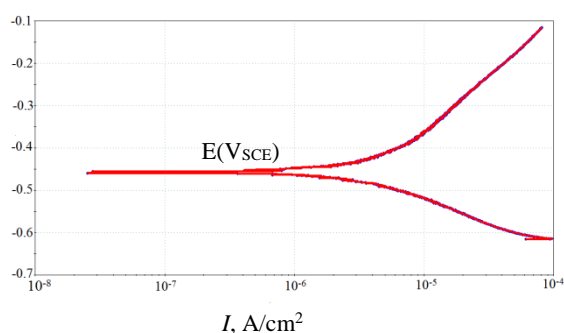


**Fig. 8.** Polarization curves for bulk  $\text{Al}_{0.4}\text{FeCrCo}_{1.5}\text{NiTi}_{0.3}$  HEA after SPS

From the observed corrosion behavior it can be concluded that the passive film covers the total surface and the formation of the corrosion pits is due to the gas evolution phenomenon.

The average corrosion rates of the bulk  $\text{Al}_{0.4}\text{FeCrCo}_{1.5}\text{NiTi}_{0.3}$  alloy in 1 mol/L NaOH solution for 50 days' immersion tests at 25 °C were determined using the weight loss method. The average corrosion rate was calculated using the following formula [18]:

$$Cr = \frac{8.76 \times 10^4 \times W}{T \times A \times DN}, \quad (8)$$

where  $C_r$  is corrosion rate (in mm/year);  $W$  is the total weight loss (in g) after exposure time  $T$  (in h);  $DN$  is the density of alloy (in  $\text{g}\cdot\text{cm}^{-3}$ );  $A$  is the specimen area (in  $\text{cm}^2$ ). For  $\text{Al}_{0.4}\text{FeCrCo}_{1.5}\text{NiTi}_{0.3}$  alloy,  $DN = 8.15$ . The average corrosion rate of bulk  $\text{Al}_{0.4}\text{FeCrCo}_{1.5}\text{NiTi}_{0.3}$  alloy in 1 mol/L NaOH solution for the 50-day immersion test at 25 °C was  $2.32 \times 10^{-4}$  mm/year. The potentiodynamic polarization curves for bulk  $\text{Al}_{0.4}\text{FeCrCo}_{1.5}\text{NiTi}_{0.3}$  alloys in 1 mol/L NaOH solution are depicted in Fig. 8. The corrosion potential and current density for bulk  $\text{Al}_{0.4}\text{FeCrCo}_{1.5}\text{NiTi}_{0.3}$  alloy were  $-0.46V_{\text{SCE}}$  and  $6.85 \times 10^{-7} \text{ A cm}^{-2}$ , respectively. The low corrosion potential and current density may be attributable to surface passivation, which resulted in the excellent corrosion resistance ( $2.32 \times 10^{-4}$  mm/year) of the alloy under study.

#### 4. CONCLUSIONS

$\text{Al}_{0.4}\text{FeCrCo}_{1.5}\text{NiTi}_{0.3}$  high-entropy alloy with ultra-fine grains and an fcc structure was synthesized successfully by the MA and SPS technologies. A supersaturated solid solution containing both fcc and bcc structures was clearly observed after the MA treatment, while after SPS the bcc structures were transformed into the fcc type. SEM analysis results showed that the obtained HEA contained nanostructures, whereas the TEM analysis results strongly suggested that the bulk  $\text{Al}_{0.4}\text{FeCrCo}_{1.5}\text{NiTi}_{0.3}$  HEA consisted mainly of Co–Ni–Fe–Cr-rich fcc phase, with minor Ti and Al-enriched bcc and  $\text{TiAl}_3$  phases. Moreover, nanoscale twins in partial fcc phase were observed in the studied HEA wherein the matrix axis was  $[011]_M$  and the twin axis was  $[0\bar{1}\bar{1}]_r$ . The compressive strength, compression ratio and Vickers hardness of  $\text{Al}_{0.4}\text{FeCrCo}_{1.5}\text{NiTi}_{0.3}$  HEA were  $2225 \pm 15$  MPa,  $17.52 \pm 0.50\%$  and  $515 \pm 16$  HV, respectively. Furthermore, the corrosion potential and current density

measurements of the as-prepared HEA corroborated its excellent corrosion resistance characteristics.

#### Acknowledgements

This study was supported by Jiangsu Provincial Natural Science Foundation of China (BK20151461), National Natural Science Foundation of China (51671104, 51601089), the Opening Project of Guangdong Key Laboratory for Advanced Metallic Materials Processing (South China University of Technology (GJ201610), Outstanding Scientific and Technological Innovation Team in Colleges and Universities of Jiangsu Province, and the Jian-gsu student platform for innovation and entrepreneurship training program (201611276004).

#### REFERENCES

1. **Yeh, J.W., Chang, S.Y., Hong, Y.D., Chen, S.K., Lin, S.J.** Anomalous Decrease in X-ray Diffraction Intensities of Cu-Ni-Al-Co-Cr-Fe-Si Alloy Systems with Multi-principal Elements *Materials Chemistry and Physics* 103 2007: pp. 41–46. <https://doi.org/10.1016/j.matchemphys.2007.01.003>
2. **Tsai, K.Y., Tsai, M.H., Yeh, J.W.** Sluggish Diffusion in Co-Cr-Fe-Mn-Ni High Entropy Alloys *Acta Materials* 61 2013: pp. 4887–4897. <http://dx.doi.org/10.1016/j.actamat.2013.04.058>
3. **Jiang, L., Lu, Y., Dong, Y., Wang, T., Cao, Z., Li, T.** Annealing Effects on the Microstructure and Properties of Bulk High-entropy CoCrFeNiTi0.5 Alloy Casting Ingots *Intermetallics* 44 2014: pp. 37–43. <https://doi.org/10.1016/j.intermet.2013.08.016>
4. **Varalakshmi, S., Kamaraj, M., Murty, B.S.** Synthesis and Characterization of Nanocrystalline AlFeTiCrZnCu High Entropy Solid Solution by Mechanical Alloying *Journal of Alloys and Compounds* 460 2008: pp. 253–257. <https://doi.org/10.1016/j.jallcom.2007.05.104>
5. **Yang, X., Zhang, Y.** Prediction of High-entropy Stabilized Solid-solution in Multi-component Alloys *Materials Chemistry and Physics* 132 2012: pp. 233–238. <https://doi.org/10.1016/j.matchemphys.2011.11.021>
6. **Fu, Z.Q., Chen, W.P., Xiao, H.Q., Zhou, L.W., Zhu, D.Z., Yang, S.F.** Fabrication and Properties of Nanocrystalline Co0.5FeNiCrTi0.5 High Entropy Alloy by MA-SPS Technique *Materials and Design* 44 2013: pp. 535–539. <https://doi.org/10.1016/j.matdes.2012.08.048>
7. **Chen, Y.L., Hu, Y.H., Hsieh, C.A., Yeh, J.W., Chen, S.K.** Competition between Elements during Mechanical Alloying in an Octonary Multi-principal-Element Alloy System *Journal of Alloys and Compounds* 481 2009: pp. 769–775. <https://doi.org/10.1016/j.jallcom.2009.03.087>
8. **Varalakshmi, S., Appa Rao, G., Kamaraj, M., Murty, B.S.** Hot Consolidation and Mechanical Properties of Nanocrystalline Equiatomic AlFeTiCrZnCu High Entropy Alloy after Mechanical Alloying *Journal of Materials Science* 45 2010: pp. 5158–5163. <https://doi.org/10.1007/s10853-010-4246-5>
9. **Yang, X., Zhang, Y.** Prediction of High-entropy Stabilized Solid-solution in Multicomponent Alloys *Materials Chemistry and Physics* 132 2012: pp. 233–238.

<https://doi.org/10.1016/j.matchemphys.2011.11.021>

10. **Zhang, Y., Zuo, T.T., Tang, Z., Gao, M.C., Dahmen, A., Liaw, P.K., Lu, Z.P.** Microstructures and Properties of High-entropy Alloys *Progress in Materials Science* 61 2014: pp. 1–93.  
<http://dx.doi.org/10.1016/j.pmatsci.2013.10.001>
11. **Guo, S., Liu, C.T.** Phase Stability in High Entropy Alloys: Formation of Solid Solution Phase or Amorphous Phase *Progress in Natural Science Materials International* 21 2011: pp. 433–446.  
<https://doi.org/10.1016/j.intermet.2013.05.002>
12. **Otto, F., Hanold, N.L., George, E.P.** Microstructural Evolution after Thermomechanical Processing in an Equi-atomic, Single-phase CoCrFeMnNi High-entropy Alloy with Special Focus on Twin Boundaries *Intermetallics* 54 2014: pp. 39–48.  
<https://doi.org/10.1016/j.intermet.2014.05.014>
13. **Stepanov, N., Tikhonovsky, M., Yurchenko, N., Zyabkin, D., Klimova, M., Zhrebtsov, S., Efimov, A., Salishchev, G.** High Temperature Deformation Behavior and Dynamic Recrystallization in CoCrFeNiMn High Entropy Alloy 636 2015 :pp 188-195.  
<https://doi.org/10.1016/j.msea.2015.03.097>
14. **Fu, Z.Q., Chen, W.P., Wen, H.M, Zhang, D.L., Chen, Z., Zheng, B.L., Zhou, Y.Z., Lavernia, E.J.** Microstructure and Strengthening Mechanisms in an FCC Structured Single-phase Nanocrystalline Co25Ni25Fe25Al7.5 Cu17.5 High Entropy Alloy *Acta Materialia* 107 2016: pp. 59–71.  
<http://dx.doi.org/10.1016/j.actamat.2016.01.050>
15. **Fu, Z.Q., Chen, W.P, Fang, S.C., Li, X.M.** Effect of Cr Addition on the Alloying Behavior, Microstructure and Mechanical Properties of Twinned CoFeNiAl0.5Ti0.5 Alloy *Materials Science & Engineering A* 597 2014: pp. 204–211.  
<https://doi.org/10.1016/j.msea.2013.12.096>
16. **Fang, S.F., Chen, W.P., Fu, Z.Q.** Microstructure and Mechanical Properties of Twinned Al0.5CrFeNiCo0.3C0.2 High Entropy Alloy Processed by Mechanical Alloying and Spark Plasma Sintering *Materials and Design* 54 2014: pp. 973–979.  
<https://doi.org/10.1016/j.matdes.2013.08.099>
17. **Chen, W.P, Fu, Z.Q., Fang, S.C., Xiao, H.Q., Zhu, D.Z.** Alloying Behavior, Microstructure and Mechanical Properties in a FeNiCrCo0.3Al0.7 High Entropy Alloy *Materials and Design* 51 2013: pp. 854–860.  
<https://doi.org/10.1016/j.matdes.2013.04.061>
18. **Hsu, Y.J., Chiang, W.C., Wu, J.K.** Corrosion Behavior of FeCoNiCrCu<sub>x</sub> High-entropy Alloys in 3.5 % Sodium Chloride Solution *Materials Chemistry and Physics* 92 2005: pp. 112–117.  
<https://doi:10.1016/j.matchemphys.2005.01.001>